Probing the Sivers asymmetries through J/ψ photoproduction in $p^{\uparrow}p$ collision with forward proton tagging

Hao Sun,* Tichouk, and Xuan Luo

Institute of Theoretical Physics, School of Physics, Dalian University of Technology, No.2 Linggong Road, Dalian, Liaoning 116024, P. R. China

(Received 31 December 2018; published 8 July 2019)

In this paper we probe the Sivers asymmetries through J/ψ photoproduction in $p^{\uparrow}p$ collision within the nonrelativistic QCD framework, based on the color-octet model and the transverse-momentum-dependent parton distributions (TMDs). Both the Dokshitzer-Gribov-Lipatov-Altarelli-Parisi evolution and TMD evolution are included. The intensity and sign of the Sivers asymmetry are strongly dependent upon the evolution model used to investigate the gluon Sivers function (GSF). Sizable asymmetries are obtained as a function of the rapidity, $\log(x_\gamma)$, or $\log(x_g)$ using a recent parametrization of the GSF at the RHIC and AFTER@LHC experiments with the planned LHC forward-detector acceptances.

DOI: 10.1103/PhysRevD.100.014007

I. INTRODUCTION

Transverse spin physics can be studied in high-energy processes that involve polarized hadrons. This allows us to investigate the polarized quark and gluon structure of hadrons and provide information on the three-dimensional structure of nucleons. The study of transverse spin physics can give more details about QCD dynamics at high energy scales, therefore and is of strong interest and highly motivating.

Transverse single-spin asymmetries (SSAs) is a topic in spin physics that has drawn a lot of attention for quite some time [1,2]. SSAs appear in scattering processes when one of the colliding protons is transversely polarized and scatters off of an unpolarized proton or hadron target with respect to the scattering plane. A possible explanation for the presence of SSAs is known as the Sivers effect, was proposed many years ago [3]. It considers the nonperturbative quantum correlation between the transverse momentum of partons and the polarization vector of the nucleon, which can be described within the framework of the generalized parton model (GPM) [4,5]. In the GPM, the inclusive cross section can be written as a convolution of the QCD partonic cross sections, the transverse-momentum-dependent parton distribution functions (TMD-PDFs), and the transverse-momentum-dependent fragmentation functions (TMD-FFs), wherein the PDFs and FFs depend on the intrinsic momentum $k_\perp$ as well as the momentum fraction variable x. For more details, see references in Refs. [4–12] regarding the theoretical aspects of understanding the origin of SSAs. There has been significant experimental progress in the measurement of the Sivers effects by the HERMES [13–15], COMPASS [16–20], JLAB [21,22], and RHIC [23] collaborations. The experimental data released by these collaborations has allowed the extraction of the Sivers functions for u and d quarks [24–27]. The gluon Sivers function (GSF) has been extracted from semi-inclusive deep-inelastic scattering (SIDIS) processes, but it still remains poorly measured. An indirect estimation of the GSF exists, which was obtained in Ref. [28] within the GPM framework by fitting the midrapidity data on SSAs in π^0 production at RHIC.

The quarkonium production process is a useful tool that is used to probe gluons inside hadrons [29] through single photoproductions of J/ψ. More recently and more importantly, the study of J/ψ formation has been theoretically carried out in electron-proton [25,30–33] and proton-proton (pp) [34,35] collisions. The GSF and linearly polarized gluon distribution [36,37] have been studied at length. The mechanism of quarkonium creation out of two heavy quarks is a nonperturbative process and is treated in terms of different models, including nonrelativistic QCD (NRQCD) factorization [38] which was chosen because it has effectively explained J/ψ photoproduction at the Tevatron [39,40], along with data from J/ψ photoproduction at HERA [41–44]. In NRQCD, the production and decay of heavy quarkonium are split into two steps. To start

*haosun@mail.ustc.edu.cn; haosun@dlut.edu.cn

with, a heavy quark-antiquark pair is perturbatively built at short distances, which is obtained out by an expansion in the strong coupling constant α_s. Then, the pair nonperturbatively evolves into quarkonium at a long distance. The short-distance coefficients are calculated perturbatively by the projection technique and the long-distance matrix elements (LDMEs) are extracted from the experimental data. The LDMEs scale is expanded in powers of the typical heavy-quark (or antiquark) velocity v in the quarkonium rest frame [45]. Therefore, the NRQCD factorization can be thought of as a doubly expanded expression in terms of v as well as α_s. As a matter of fact, the asymmetry is very receptive to the production mechanism. On the one hand, in pp collisions through a γg subcollision, the final-state interactions with the heavy quark and antiquark are neutralized among themselves when the pair is produced in a color-singlet configuration, giving a zero asymmetry. On the other hand, one gets a nonzero asymmetry when the pair is produced in a color-octet configuration [46].

To follow up on the understanding of the origin of the Sivers effect, numerous theoretical studies of different key processes have been performed in the context of $ep^{\uparrow}$ collisions (such as heavy-quark pair and dijet production [33], inelastic J/ψ photoproduction [47], and $e + p^{\uparrow} \to e + J/\psi + X$ [30,48,49]), as well as $pp^{\uparrow}$ scattering (for instance, $pp^{\uparrow} \to h + X$ [50]), D-meson production [34,51], back-to-back jet correlations [52], etc. Even so, a great deal of insufficiencies have been pointed out regarding the failure of certain interactions to quantify the gluon Sivers function, which can be attributed to the problem of TMD-factorization-breaking contributions [53], some features of which have been partially probed. A plan to study standard model physics using the forward detector to allow for the search of new physics signals was suggested by the FP420 R&D Collaboration in 2009 [54]. To reach this new realm of interest, detectors in the LHC tunnel need to be readjusted so as to precisely measure very forward protons. The forward-detector equipment is relevant for the study of photoproduction processes which can exclude many serious backgrounds, and forward proton tagging could give a clean signal of new physics domains. Moreover, the proton-proton collision data would offer knowledge about unexplored phase-space areas. Three different forward-detector acceptances are given as $0.1 < \xi < 0.5$, $0.0015 < \xi < 0.5$, and $0.015 < \xi < 0.15$, and the entire range of the forward-detector acceptance without any cut is $0 < \xi < 1$. Among the hadronic collisions, the processes with one single J/ψ and one intact unpolarized hadron emitting a photon in the final state would, in any case, be a safe way [28] to measure the GSF with forward-detector acceptances. Henceforth, single heavy quarkonium productions are considered to be clean probes of the GSF.

In this paper, we delve into the possibility of utilizing single charmonium production to obtain evidence on the Sivers function with the forward-detector acceptance together with the presentation of predictions for SSAs through the process $hp^{\uparrow} \to h\gamma p^{\uparrow} \to h\mathcal{Q} + X$ where h is an unpolarized hadron (in our case, a proton). The asymmetry has been assessed by employing the NRQCD framework within the color-octet model owing to the vanishing color-octet contribution in the aforementioned pp collision. The unpolarized cross section of single J/ψ production has been calculated to estimate the denominator of SSAs. The rapidity distribution of SSAs has been estimated in Ref. [55] in Dokshitzer-Gribov-Lipatov-Altarelli-Parisi (DGLAP) evolution using the color evaporation model (CEM), and we extend this work to TMD evolution using the NRQCD approach. The $y^{J/\psi}$, $\log(x_\gamma)$, $\log(x_g)$, and $p_T^{J/\psi}$ distributions are evaluated at the forward detector in the present work and considerable asymmetries are observed in NRQCD compared to those in the CEM.

We give estimates of the asymmetry for forthcoming suggested experiments at AFTER@LHC (which is a fixed-target experiment with $\sqrt{s} = 115$ GeV) and for $\sqrt{s} = 200$, 500 GeV which will be surveyed at the RHIC with planned LHC forward-detector acceptances. Two up-to-date extractions [26,28] are used to determine the gluon Sivers function from the SSA data in pp collisions at the RHIC. The paper is structured as follows. Single J/ψ photoproduction with forward proton tagging by using NRQCD and the SSAs in DGLAP evolution along with TMD evolution are presented in Sec. II. In Sec. III, we give both the input parameters and the numerical results. Section IV is devoted to a summary and discussions.

II. CALCULATION FRAMEWORK

A. J/ψ photoproduction in $p^{\uparrow}p$ collisions with forward proton tagging

Strong electromagnetic fields are created when a charged proton (p) or charged nucleus (A) moves close to the speed of light (c). On the one hand, the photon arising from the field of one of the two ultrarelativistic and charged hadrons (p or A) can collide with one photon of the other hadron (photon-photon process). On the other hand, this photon can also directly interact with the other hadron (photon-hadron process) [55]. The total cross section of this process can be split into terms for the equivalent flux of photons into the hadron projectile and the photon-photon or photon-target cross section. At this point, the photons presumably come from the unpolarized hadron (p or A), which interacts with the transversely polarized protons at high energies, generating a J/ψ and dissociating the proton target.

In the case of $pp^{\uparrow}$ collisions, the process of interest can be separated by tagging the unpolarized proton in the final state, which is present when it emits the photon. We will consider heavy quarkonium production in the NRQCD factorization formalism. We refer to the heavy quarkonium

J/ψ as $\mathcal{Q}$. As a consequence, the hadronic cross section for the $hp^{\uparrow} \to h\gamma p^{\uparrow} \to h\mathcal{Q} + X$ process can be expressed as

$$\sigma(hp^{\uparrow} \to h\gamma p^{\uparrow} \to h\mathcal{Q} + X) = \int dx_\gamma d^2\mathbf{k}_{\perp\gamma} f_{\gamma/h}(x_\gamma, \mathbf{k}_{\perp\gamma}) dx_g d^2\mathbf{k}_{\perp g} f_{g/p^{\uparrow}}(x_g, \mathbf{k}_{\perp g}, \mu_f) \times \sum_n \hat{\sigma}(\gamma g \to Q\bar{Q}[n] + X) \langle 0|\mathcal{O}^{J/\psi}_{1,8}[n]|0\rangle, \quad (1)$$

where $\langle 0|\mathcal{O}^{J/\psi}_{1,8}[n]|0\rangle$ are the long-distance matrix elements, which describe the hadronization of the heavy pair into the physical observable quarkonium state J/ψ. $\hat{\sigma}(\gamma g \to Q\bar{Q}[n])$ denotes the short-distance cross section for the partonic process $\gamma g \to Q\bar{Q}[n]$, which is found by using the covariant projection method. The Fock states n are given as follows: ${}^1S_0^{[8]}$, ${}^3P_0^{[8]}$, ${}^3P_2^{[8]}$ for the $\gamma g \to Q\bar{Q}[n]$ partonic process. The final state (h) will be characterized by the presence of one rapidity gap and an intact hadron, which we assume to be the unpolarized one. Both aspects can be used in principle to experimentally separate the vector mesons produced by photon-induced interactions.

In our exploratory study here we will suppose that the transverse-momentum dependence of the photon distribution can be described by a simple Gaussian form:

$$f_{\gamma/h}(x_\gamma, \mathbf{k}_{\perp\gamma}) = f_{\gamma/h}(x_\gamma) \frac{1}{\pi\langle k^2_{\perp\gamma}\rangle} e^{-\mathbf{k}^2_{\perp\gamma}/\langle k^2_{\perp\gamma}\rangle}, \quad (2)$$

where x_γ is the energy fraction of the hadron carried by the photon with transverse momentum $\mathbf{k}_{\perp\gamma}$ and can be symbolized by $x_\gamma = \frac{E_\gamma}{E}$, the ratio between the scattered low-Q^2 photons E_γ and incoming energy E. $f_{\gamma/h}(\xi)$ represents the effective photon density function which is defined by the equivalent photon approximation [56,57] in our computation:

$$f_{\gamma/h}(\xi) = \int_{Q^2_{\min}}^{Q^2_{\max}} \frac{dN_\gamma(\xi)}{d\xi dQ^2} dQ^2, \quad (3)$$

where $\frac{dN_\gamma(\xi)}{d\xi dQ^2}$ is the spectrum of the quasireal photon

$$\frac{dN_\gamma(\xi)}{d\xi dQ^2} = \frac{\alpha}{\pi}\frac{1}{\xi Q^2}\left[(1-\xi)\left(1 - \frac{Q^2_{\min}}{Q^2}\right)F_E + \frac{\xi^2}{2}F_M\right] \quad (4)$$

with

$$Q^2_{\min} = \frac{m_p^2\xi^2}{1-\xi}, \qquad F_E = \frac{4m_p^2 G_E^2 + Q^2 G_M^2}{4m_p^2 + Q^2},$$
$$G_E^2 = \frac{G_M^2}{\mu_p^2} = \left(1 + \frac{Q^2}{Q_0^2}\right)^{-4}, \qquad F_M = G_M^2, \quad (5)$$

where α is the fine-structure constant, $\mu_p^2 = 7.78$ is the magnetic moment of the proton, $Q_0^2 = 0.71$ GeV^2, m_p is its mass, the value of $Q^2_{\max}$ is around 2 GeV^2, and ξ represents x_γ. $f_{g/p^{\uparrow(\downarrow)}}(x_g, \mathbf{k}_{\perp g}, \mu_f)$ stands for the number density of gluons with light-cone momentum fraction x_g and transverse momentum $\mathbf{k}_{\perp g} = k_{\perp g}(\cos\phi_a, \sin\phi_a)$ inside the transversely polarized proton. The polarization of the proton is up or down with respect to the production plane, moving along the $\hat{z}$ axis. Considering the partonic process $\gamma(p_1) + g(p_2) \to Q\bar{Q}[n](p_3)$, the final total cross section for the $hp^{\uparrow} \to h\gamma p^{\uparrow} \to h\mathcal{Q} + X$ process can be expressed as

$$\sigma(hp^{\uparrow} \to h\gamma p^{\uparrow} \to h\mathcal{Q} + X) = \int \frac{\pi}{s^2 x_g x_\gamma^2}\frac{1}{N_{\rm col}N_{\rm pol}}\overline{\sum}|\mathcal{A}_{S,L}|^2 f_{\gamma/h}(x_\gamma, \mathbf{k}_{\perp\gamma}) \times f_{g/p^{\uparrow}}(x_g, \mathbf{k}_{\perp g}, \mu))\langle 0|\mathcal{O}^{J/\psi}_{1,8}[n]|0\rangle d^2\mathbf{p}_3 dx_\gamma d^2\mathbf{k}_{\perp\gamma}, \quad (6)$$

with x_g fixed by $x_g = m_{3T}^2/(sx_\gamma)$ and $\mathbf{k}_{\perp\gamma}$ fixed by $\mathbf{p}_{3T} - \mathbf{k}_{\perp g}$. Here x_γ is integrated in the region $x_{\gamma\,\min} < x_\gamma < x_{\gamma\,\max}$ and $x_{\gamma\,\min}$ ($x_{\gamma\,\max}$) is the lower (upper) limit of forward-detector acceptance. m_T is the transverse mass of the particle, defined as $m_T = \sqrt{m^2 + p_T^2}$. s and m are, respectively, the square of the center-of-mass energy of the collider and the mass of the particle. Similarly as in photoproduction induced by electron-proton collisions, we can define the z parameter $z = P_h \cdot P_3/P_h \cdot q_\gamma$ where P and q_γ are the momenta of the proton and virtual photon, respectively. The data is taken in the elastic regime for the $\gamma g \to Q\bar{Q}[n]$ partonic process. Conversely, the inelastic regime is commonly considered to be the area where z is below 0.8 or 0.9. The elastic regime is considered to be the area near $z = 1$, which is exactly where we concentrate for our study of J/ψ production.

The summation in Eq. (6) is taken over the spins and colors of initial and final states, and the bar over the summation denotes averaging over the spins and colors of the initial parton. $N_{\rm col}$ and $N_{\rm pol}$ refer to the number of colors and polarizations of states n, respectively. In the notation of Ref. [58], we have

$$\mathcal{A}_{Q\bar{Q}}[{}^1S_0^{(1/8)}] = \mathrm{Tr}[\mathcal{C}_{(1/8)}\Pi_0\mathcal{A}]_{q=0},$$
$$\mathcal{A}_{Q\bar{Q}}[{}^3S_1^{(1/8)}] = \epsilon_\alpha \mathrm{Tr}[\mathcal{C}_{(1/8)}\Pi_1^\alpha\mathcal{A}]_{q=0},$$
$$\mathcal{A}_{Q\bar{Q}}[{}^1P_1^{(1/8)}] = \epsilon_\beta \frac{d}{dq_\beta}\mathrm{Tr}[\mathcal{C}_{(1/8)}\Pi_0\mathcal{A}]_{q=0},$$
$$\mathcal{A}_{Q\bar{Q}}[{}^1P_J^{(1/8)}] = \epsilon^{(J)}_{\alpha\beta}\frac{d}{dq_\beta}\mathrm{Tr}[\mathcal{C}_{(1/8)}\Pi_1^\alpha\mathcal{A}]_{q=0}, \quad (7)$$

where $\mathcal{A}$ denotes the QCD amplitude with amputated heavy-quark spinors, and the lower index q represents the momentum of the heavy quark in the $Q\bar{Q}$ rest frame. $\Pi_{0/1}$ are spin projectors onto spin-singlet and spin-triplet states,

$$\Pi_0 = \frac{1}{\sqrt{8m^3}}\left(\frac{\not{P}}{2} - \not{q} - m\right)\gamma_5\left(\frac{\not{P}}{2} + \not{q} + m\right),$$
$$\Pi_1^\alpha = \frac{1}{\sqrt{8m^3}}\left(\frac{\not{P}}{2} - \not{q} - m\right)\gamma^\alpha\left(\frac{\not{P}}{2} + \not{q} + m\right), \quad (8)$$

where P is the total momentum of the heavy quarkonium, q is the relative momentum between the $Q\bar{Q}$ pair, and m_Q is the mass of the heavy quark. $\mathcal{C}_{1/8}$ are color-factor projectors onto the color-singlet and color-octet states and can be expressed as follows:

$$C_1 = \frac{\delta_{ij}}{\sqrt{N_c}},$$
$$C_8 = \sqrt{2}T^c_{ij}, \quad (9)$$

where N_c is the number of colors, and T^c_{ij} is the generator of $SU(N_c)$. The summation over the polarization is given as

$$\sum_{J_z}\varepsilon_\alpha\varepsilon^*_{\alpha'} = \Pi_{\alpha\alpha'},$$
$$\sum_{J_z}\varepsilon^0_{\alpha\beta}\varepsilon^{0*}_{\alpha'\beta'} = \frac{1}{3}\Pi_{\alpha\beta}\Pi_{\alpha'\beta'},$$
$$\sum_{J_z}\varepsilon^1_{\alpha\beta}\varepsilon^{1*}_{\alpha'\beta'} = \frac{1}{2}(\Pi_{\alpha\alpha'}\Pi_{\beta\beta'} - \Pi_{\alpha\beta'}\Pi_{\alpha'\beta}),$$
$$\sum_{J_z}\varepsilon^2_{\alpha\beta}\varepsilon^{2*}_{\alpha'\beta'} = \frac{1}{2}(\Pi_{\alpha\alpha'}\Pi_{\beta\beta'} + \Pi_{\alpha\beta'}\Pi_{\alpha'\beta}) - \frac{1}{3}\Pi_{\alpha\beta}\Pi_{\alpha'\beta'}, \quad (10)$$

where ε_α ($\varepsilon_{\alpha\beta}$) represents the polarization vector (tensor) of the $Q\bar{Q}$ states, $\Pi_{\alpha\beta} = -g_{\alpha\beta} + \frac{P_\alpha P_\beta}{M^2}$, and M is the heavy quarkonium mass. The squared amplitudes for $2 \to 1$ partonic processes are presented as follows [59]:

$$\overline{\sum}|\mathcal{M}[^{2S+1}L_J^{[1,8]}]|^2 = \frac{1}{N_{\rm col}N_{\rm pol}}\overline{\sum}|\mathcal{A}_{S,L}|^2, \quad (11)$$

where

$$\overline{\sum}|\mathcal{M}[^1S_0^{[8]}]|^2 = \frac{(4\pi)^2\alpha\alpha_s e_c^2}{2M},$$
$$\overline{\sum}|\mathcal{M}[^3P_0^{[8]}]|^2 = \frac{6(4\pi)^2\alpha\alpha_s e_c^2}{M^3},$$
$$\overline{\sum}|\mathcal{M}[^3P_2^{[8]}]|^2 = \frac{8(4\pi)^2\alpha\alpha_s e_c^2}{5M^3}. \quad (12)$$

At low $p_T^{J/\psi}$, the heavy quarkonia is dominantly produced at high-energy colliders via the color-octet channel. Finally, we have

$$|\overline{\mathcal{M}}|^2 = (4\pi)^2 e_c^2\alpha\alpha_s\left(\frac{1}{2M}\langle 0|\mathcal{O}_8^{J/\psi}(^1S_0)|0\rangle + \frac{6}{M^3}\langle 0|\mathcal{O}_8^{J/\psi}(^3P_0)|0\rangle + \frac{8}{5M^3}\langle 0|\mathcal{O}_8^{J/\psi}(^3P_2)|0\rangle\right). \quad (13)$$

B. Sivers asymmetry and parametrization in DGLAP evolution

The transverse SSA for the process $h + p^\uparrow \to J/\psi + X$ is defined by

$$A_N = \frac{d\sigma^\uparrow - d\sigma^\downarrow}{d\sigma^\uparrow + d\sigma^\downarrow} = \frac{d\Delta\sigma}{2d\sigma}, \quad (14)$$

where $d\sigma^{\uparrow(\downarrow)}$ denotes the single-polarized cross section, in which one of the protons in the initial state is polarized along the transverse direction $\uparrow(\downarrow)$ with respect to the production plane. One has that the cross section for J/ψ photoproduction is proportional to the number density of gluons inside a proton with transverse polarization $\mathbf{S}_\perp$ and momentum $\mathbf{P}$. We choose the frame where the polarized proton is moving along the z axis with momentum $\mathbf{P}$ and is transversely polarized with $\mathbf{S}_\perp = S_\perp(\cos\phi_s, \sin\phi_s, 0)$. For a general value of the transverse spin $\mathbf{S}_\perp$, it is parametrized in terms of the GSF $\Delta^N f_{g/p^\uparrow}$ as follows:

$$f_{g/p^\uparrow}(x_g, \mathbf{k}_{\perp g}, \mathbf{S}_\perp, \mu) = f_{g/p}(x_g, k_{\perp g}, \mu) + \frac{1}{2}\Delta^N f_{g/p^\uparrow}(x_g, k_{\perp g}, \mu)\hat{\mathbf{S}}_\perp\cdot(\hat{\mathbf{P}}\times\hat{\mathbf{k}}_{\perp g}), \quad (15)$$

where $f_{g/p}(x_g, k_{\perp g}, \mu)$ is the unpolarized TMD gluon distribution. It is generally assumed that the unpolarized gluon TMDs obey the Gaussian distribution at low-PT. The spectra appear to have a Gaussian shape. The Gaussian parametrization of an unpolarized TMD [24] that is commonly and phenomenologically used is given by

$$f_{g/p}(x_g, \mathbf{k}_{\perp g}, \mu) = f_{g/p}(x_g, \mu)\frac{1}{\pi\langle k_\perp^2\rangle}e^{-k_\perp^2/\langle k_\perp^2\rangle}. \quad (16)$$

Here $f_{g/p}(x_g, \mu)$ is the normal collinear PDF, which is measured at the scale μ. The collinear PDF obeys the DGLAP scale evolution. There is no evolution for a normalized Gaussian in the transverse momenta $k_\perp$. The transverse momentum of the initial gluon is $\mathbf{k}_{\perp g} = k_{\perp g}(\cos\phi_g, \sin\phi_g, 0)$, so that $\hat{\mathbf{S}}_\perp\cdot(\hat{\mathbf{P}}\times\hat{\mathbf{k}}_{\perp g}) = \sin(\phi_g - \phi_s)$. For numerical estimation we can take $\phi_s = \pi/2$. By considering Eq. (6), we can write the numerator and denominator of Eq. (14) as

$$\frac{d\sigma^{\uparrow}}{d^2\mathbf{p}_3}-\frac{d\sigma^{\downarrow}}{d^2\mathbf{p}_3}=\int dx_\gamma d^2\mathbf{k}_{\perp\gamma} f_{\gamma/h}(x_\gamma,\mathbf{k}_{\perp\gamma})[f_{g/p^{\uparrow}}(x_g,\mathbf{k}_{\perp g},\mu)-f_{g/p^{\downarrow}}(x_g,\mathbf{k}_{\perp g},\mu)]\frac{\pi}{s^2x_gx_\gamma^2}|\overline{\mathcal{M}}|^2\sin(\phi_3-\phi_s),$$
$$\frac{d\sigma^{\uparrow}}{d^2\mathbf{p}_3}+\frac{d\sigma^{\downarrow}}{d^2\mathbf{p}_3}=2\int dx_\gamma d^2\mathbf{k}_{\perp\gamma} f_{\gamma/h}(x_\gamma,\mathbf{k}_{\perp\gamma})f_{g/p}(x_g,\mathbf{k}_{\perp g})\frac{\pi}{s^2x_gx_\gamma^2}|\overline{\mathcal{M}}|^2, \tag{17}$$

where $\sin(\phi_3-\phi_s)$ is a weighted factor and ϕ_3 and ϕ_s are the azimuthal angles of the J/ψ and proton spin, respectively.

We also have

$$\Delta^N f_{g/p^{\uparrow}}(x_g,\mathbf{k}_{\perp g},\mu)=[f_{g/p^{\uparrow}}(x_g,\mathbf{k}_{\perp g},\mu)-f_{g/p^{\downarrow}}(x_g,\mathbf{k}_{\perp g},\mu)]=\Delta^N f_{g/p^{\uparrow}}(x_g,k_{\perp g},\mu)\hat{\mathbf{S}}_\perp\cdot(\hat{\mathbf{P}}\times\hat{\mathbf{k}}_{\perp g}). \tag{18}$$

The parametrization of the gluon Sivers function can be described in the well-known Gaussian-like format as follows:

$$\Delta^N f_{g/p^{\uparrow}}(x_g,k_{\perp g},\mu)=2N_g(x_g)f_{g/p}(x_g,\mu)h(k_{\perp g})\frac{e^{-k_{\perp g}^2/\langle k_{\perp g}^2\rangle}}{\pi\langle k_{\perp g}^2\rangle}, \tag{19}$$

where

$$\mathcal{N}_g(x_g)=N_g x_g^{\alpha}(1-x_g)^{\beta}\frac{(\alpha+\beta)^{\alpha+\beta}}{\alpha^{\alpha}\beta^{\beta}} \tag{20}$$

with $|N_g|\le 1$ and

$$h(k_{\perp g})=\sqrt{2e}\frac{k_{\perp g}}{M_1}e^{-k_{\perp g}^2/M_1^2}. \tag{21}$$

Therefore, the $k_{\perp g}$-dependent part of the Sivers function can be expressed as follows:

$$h(k_{\perp g})\frac{e^{-k_{\perp g}^2/\langle k_{\perp g}^2\rangle}}{\pi\langle k_{\perp g}^2\rangle}=\frac{\sqrt{2e}}{\pi}\sqrt{\frac{1-\rho}{\rho}}k_{\perp g}\frac{e^{-k_{\perp g}^2/\rho\langle k_{\perp g}^2\rangle}}{\langle k_{\perp g}^2\rangle^{3/2}}, \tag{22}$$

where

$$\rho=\frac{M_1^2}{\langle k_{\perp g}^2\rangle+M_1^2}. \tag{23}$$

Here N_g, α,β, and M_1 are all parameters determined by fits to data and e is Euler's number. The two extractions of the GSF, namely, SIDIS1 and SIDIS2, were obtained by fitting to data. The numerical values of the free parameters a_f, b_f, and N_f have been estimated by a global fit of single-spin asymmetry in SIDIS processes [26,28]. However, only the u and d quarks' free parameters are extracted [24] and the gluon parameters a_g, b_g, and N_g are not known yet. To estimate SSAs we use two parametrizations to attain the best-fit parameters of the gluon Sivers function [52],

$$\text{(a) } \mathcal{N}_g(x)=\frac{\mathcal{N}_u(x)+\mathcal{N}_d(x)}{2},$$
$$\text{(b) } \mathcal{N}_g(x)=\mathcal{N}_d(x). \tag{24}$$

The best-fit parameters are tabulated in the following section.

The above simplified expression, which we adopt for both the unpolarized distribution and the Sivers function, is known as the Gaussian factorization ansatz. It has been favorably checked against the data in Drell-Yan [60] and SIDIS processes [61]. However, it is still far less clear whether it is a suitable method to the study DGLAP evolution of TMDs. The factorization ansatz, which is assumed to hold at an initial condition scale, is broken at higher scales and the breaking increases with the evolution range and with decreasing x [62]. In particular, it is completely broken in the very low-x limit [63]. It was also found that the DGLAP evolution approach may not be able to describe the Z-boson high transverse momentum distribution in Drell-Yan processes at CDF [64]. Nevertheless, to also explain high-P_T data one has to consider the TMD evolution approach, which we will study in the following subsection.

The final expressions for the asymmetries can be written in the DGLAP evolution formalism. By considering the $\sin(\phi_3-\phi_s)$ weighted factor, the numerator and denominator terms of Eq. (14) are given by

$$\frac{d\sigma^{\uparrow}}{d^2\mathbf{p}_3}-\frac{d\sigma^{\downarrow}}{d^2\mathbf{p}_3}=\int dx_\gamma d^2\mathbf{k}_{\perp\gamma} f_{\gamma/h}(x_\gamma,\mathbf{k}_{\perp\gamma}) f_{g/p}(x_g,\mu) \times 2N_g(x)\frac{\sqrt{2e}}{\pi}\sqrt{\frac{1-\rho}{\rho}}k_{\perp g}\frac{e^{-k_{\perp g}^2/\rho\langle k_{\perp g}^2\rangle}}{\langle k_{\perp g}^2\rangle^{3/2}}\frac{\pi}{s^2x_g x_\gamma^2}|\overline{\mathcal{M}}|^2\sin(\phi_{\perp g}-\phi_s)\sin(\phi_3-\phi_s),$$

$$\frac{d\sigma^{\uparrow}}{d^2\mathbf{p}_3}+\frac{d\sigma^{\downarrow}}{d^2\mathbf{p}_3}=2\int dx_\gamma d^2\mathbf{k}_{\perp\gamma} f_{\gamma/h}(x_\gamma,\mathbf{k}_{\perp\gamma}) f_{g/p}(x_g,\mu)\frac{1}{\pi\langle k_{\perp g}^2\rangle}e^{-k_{\perp g}^2/\langle k_{\perp g}^2\rangle}\frac{\pi}{s^2x_g x_\gamma^2}|\overline{\mathcal{M}}|^2. \tag{25}$$

C. Sivers asymmetry and parametrization in TMD evolution

Here, we study the TMD evolution approach. Since TMDs depend on various energy scales, the TMD-PDF $f(x,k_\perp,Q)$ is best described through its Fourier transform into coordinate space (an impact parameter $b_\perp$ space), which is given by

$$f(x,b_\perp,Q)=\int d^2\mathbf{k}_\perp e^{-i\mathbf{k}_\perp\cdot\mathbf{b}_\perp}f(x,k_\perp,Q), \tag{26}$$

with the inverse Fourier transformation

$$f(x,k_\perp,Q)=\frac{1}{(2\pi)^2}\int d^2\mathbf{b}_\perp e^{i\mathbf{k}_\perp\cdot\mathbf{b}_\perp}f(x,b_\perp,Q). \tag{27}$$

The evolution of $b_\perp$-space TMD-PDFs can then be written as

$$f(x,b_\perp,Q_f)=f(x,b_\perp,Q_i)\times R_P(Q_f,Q_i,b_*) \times R_{\rm NP}(Q_f,Q_i,b_\perp), \tag{28}$$

where R_P is the perturbatively calculable part of the evolution kernel in the small-$b_\perp$ region, and $R_{\rm NP}$ is a nonperturbative Sudakov factor in the large-$b_\perp$ region (probably obtained from the experimental data [65,66]). To combine these regions, a matching procedure is introduced with a parameter $b_{\perp\max}$ serving as the boundary between the two regions. Several different prescriptions have appeared in the literature [67,68]. Here we adopt the original Collins-Soper-Sterman (CSS) prescription [69–71],

$$b_*=b_\perp/\sqrt{1+(b_\perp/b_{\perp\max})^2},\quad b_{\perp\max}<1/\Lambda_{\rm QCD}, \tag{29}$$

which allows a smooth transition from perturbative to nonperturbative regions and avoids the Landau pole singularity in $\alpha_s(\mu_{b_\perp})$. The typical value of $b_{\perp\max}$ is chosen around 1 GeV^{-1} to guarantee that b_* is always in the perturbative region.

In the small-$b_\perp$ region, the TMD distributions at fixed energy can be expressed as the convolution of the perturbatively calculable coefficients and the corresponding collinear PDFs or the multiparton correlation functions. Following Refs. [72,73], we choose an initial scale $Q_i=c/b_*$ to start the TMD evolution, where $c=2e^{-\gamma_E}$ and $\gamma_E\approx 0.577$ is the Euler-Mascheroni constant. Setting $Q_i=c/b_*$ and $Q_f=Q$, the perturbative evolution kernel is given by [72,74–79]

$$R_P(Q_f,Q_i,b_*)=\exp\left\{-\int_{c/b_*}^{Q_f}\frac{d\mu'}{\mu'}\left(A(\alpha_s(\mu'))\ln\left(\frac{Q_f^2}{\mu'^2}\right)+B(\alpha_s(\mu'))\right)\right\}\times\left(\frac{Q_f^2}{Q_i^2}\right)^{-D(b;Q_i)}, \tag{30}$$

where $A=\Gamma_{\rm cusp}$ and $B=\gamma^V$, with $\frac{dD}{d\log\mu}=\Gamma_{\rm cusp}$. $\Gamma_{\rm cusp}$ and γ^V are anomalous dimensions and can be expanded in perturbative series of α_s/π,

$$A=\sum_{n=1}^{\infty}\left(\frac{\alpha_s}{\pi}\right)^n A_n,\quad B=\sum_{n=1}^{\infty}\left(\frac{\alpha_s}{\pi}\right)^n B_n,\quad D=\sum_{n=1}^{\infty}\left(\frac{\alpha_s}{\pi}\right)^n D_n. \tag{31}$$

The expansion coefficients with the appropriate gluon anomalous dimensions up to next-to-leading-logarithmic (NLL) accuracy are [72,75,80–82]

$$A_1=C_A,\quad A_2=\frac{1}{2}C_A\left(C_A\left(\frac{67}{18}-\frac{\pi^2}{6}\right)-\frac{10}{9}T_R N_f\right),\quad B_1=-\frac{1}{2}\left(\frac{11}{3}C_A-\frac{4}{3}T_R N_f+C_A\delta_{c,8}\right),\quad D_1=\frac{C_A}{2}\log\frac{Q_i^2b_*^2}{c^2}. \tag{32}$$

The Kronecker delta $\delta_{c,8}$ derives from the interference of the initial- and final-state soft gluon radiation in the color-octet channel ($c=8$) and is absent in the color-singlet channel ($c=1$) [83]. The D term vanishes at NLL order by choosing the initial scale $Q_i=c/b_*$.

The CSS resummation formalism suggests that the nonperturbative functional is universal. Its role is similar to that of the parton distribution function in any fixed-order perturbative calculation, its origin is due to the long-distance effects that are incalculable at present, and its value must be determined from data. The general formula for the nonperturbative function is given by

$$R_{ij}^{\rm NP}(b_\perp,Q,x_A,x_B)=\exp[-\ln(Q^2/Q_0^2)g_1(b_\perp) - g_{i/A}(x_A,b_\perp)-g_{j/B}(x_B,b_\perp)], \tag{33}$$

where the functions $g_1(b_\perp)$, $g_{i/A}(x_A,b_\perp)$, and $g_{j/B}(x_B,b_\perp)$ must be extracted from data with the constraint that $R_{ij}^{\rm NP}(0,Q,x_A,x_B)=1$. They should go to zero as $b_\perp\to 0$. x_A and x_B represent the longitudinal momentum fractions of the incoming hadrons carried by the initial-state partons (photon and gluon). The $\ln(Q^2/Q_0^2)g_1(b_\perp)$ dependence comes from the infrared renormalon contributions which is a certain pattern of perturbative expansions related to the small- and large-momentum behavior [84]. Moreover, $g_1(b_\perp)$ only depends on Q, whereas $g_{i/A}(x_A,b_\perp)$ and $g_{j/B}(x_B,b_\perp)$ in general depend on x_A or x_B, and their values can depend on the flavor of the initial-state partons. The nonperturbative element of the evolution kernel cannot be evaluated and a parametrized form has to be selected. There are many extractions for the nonperturbative part mentioned in literature inspired by Refs. [65,70] which are widely used to parametrize $R_{ij}^{\rm NP}(b_\perp,Q,x_A,x_B)$ for TMD distributions. Four often-used types of functional forms are defined as follows.

(1) The nonperturbative distribution introduced by Davies, Webber, and Stirling (DWS) [85] is given by

$$R_{\rm NP}^{\rm DWS}(b_\perp,Q,x_A,x_B)=\exp[-b_\perp^2(g_1+g_2\ln(Q^2/2Q_0^2))], \tag{34}$$

where g_1 and g_2 are flavor-independent fitting parameters. The DWS distribution has a pure Gaussian form. The CSS b-space resummation formalism with the DWS distribution offers a reasonable description of the Drell-Yan data from Fermilab experiment E288 at $\sqrt{s}=27.4$ GeV [86] and CERN ISR experiment R209 at $\sqrt{s}=67$ GeV [87,88].

(2) To incorporate a possible $\ln(x_Ax_B)$ dependence that is linear in $b_\perp$, Landinsky and Yuan (LY) [89,90] suggested a revised functional form for $R_{ij}^{\rm NP}$ with an extra parameter g_3. The LY distribution is able to fit the R209 Drell-Yan data and CDF data on W and Z production from Fermilab and is given by

$$R_{\rm NP}^{\rm LY}(b_\perp,Q,x_A,x_B)=\exp[-b_\perp^2(g_1+g_2\ln(Q^2/2Q_0^2)) + b_\perp g_1g_3\ln(100x_Ax_B)]. \tag{35}$$

The LY distribution does not have a pure Gaussian form.

(3) Brock-Landry-Nadolsky-Yuan (BLNY) [64,90] performed a much more extensive global fit to the low-energy Drell-Yan data along with high-energy W and Z data by using both the DWS and LY parametrizations. The BLNY distribution is given by

$$R_{\rm NP}^{\rm BLNY}(b_\perp,Q,x_A,x_B)=\exp[-b_\perp^2(g_1+g_2\ln(Q^2/2Q_0^2) + g_1g_3\ln(100x_Ax_B))]. \tag{36}$$

The LBLY distribution also has a pure Gaussian form.

(4) Recently, the nonperturbative form factor $R_{ij}^{\rm NP}$ of BLNY associated with the unpolarized TMD-PDF of the proton was simplified. The updated BLNYs (UBLNYs) [64,83,91–93] are constructed and fitted so as to describe the low-energy SIDIS and high-energy Drell-Yan and Z production data. They can establish the universality property of the TMD distributions between DIS and Drell-Yan processes [93]. The UBLNY in Ref. [64] was chosen and used in Ref. [93] to study the unpolarized pp Drell-Yan process,

$$R_{\rm NP}^{\rm UBLNY}(b_\perp,Q,x_A,x_B)=\exp\left\{-\left[g_1b_\perp^2+g_2\ln\frac{b_\perp}{b_*}\ln\frac{Q}{Q_0} + g_3b_\perp^2\left(\left(\frac{x_0}{x_A}\right)^\lambda+\left(\frac{x_0}{x_B}\right)^\lambda\right)\right]\right\}. \tag{37}$$

With the parametrization in Table I, Eq. (37) is reduced to

$$R_{\rm NP}^{\rm UBLNY}(b_\perp,Q,x_A,x_B)=\exp\left\{-\left[\frac{g_1}{2}b_\perp^2+\frac{g_2}{2}\ln\frac{b_\perp}{b_*}\ln\frac{Q}{Q_0}\right]\right\}, \tag{38}$$

which has been used for all quark TMD-PDFs. In the case of gluon TMD-PDFs, g_2 should be multiplied by a factor of C_A/C_F. In comparison to the quark parametrization, the coefficient of the term proportional to $\ln(Q)$ is enhanced by a color factor, while the intrinsic part is kept unchanged [94].

Combining the previous discussions and following Ref. [72], one can expand the TMD $f(x,b_\perp Q)$ at the initial scale in terms of its corresponding collinear function and keep only the leading-order term, which is just the

TABLE I. Best-fit parameters of the nonperturbative Sudakov factor $R_{\rm NP}$.

$R_{\rm NP}$	g_1/GeV^2	g_2/GeV^2	g_3/GeV^2	Q_0/GeV	$b_{\max}/\mathrm{GeV}^{-1}$	x_0	λ
DWS	0.15	0.4		2	0.5		
LY	0.11	0.58	−1.5	1.6	0.5		
BLNY	0.21	0.68	−0.12	1.6	0.5		
UBLNY	0.212	0.84	0.0	1.5	1.5	0.01	0.2

collinear PDF. The TMD evolution equation of the unpolarized gluon TMD-PDF in terms of the collinear PDF in $b_\perp$ space is finally given by

$$f_{g/p}(x_g, b_\perp, Q) = f_{g/p}(x_g, c/b_*) \times \exp\left\{-\int_{c/b_*}^{Q} \frac{d\mu'}{\mu'}\left(A\ln\left(\frac{Q^2}{\mu'^2}\right)+B\right)\right\} \times \exp\left\{-\left[\frac{g_1}{2}b_\perp^2+\frac{g_2}{2}\ln\frac{b_\perp}{b_*}\ln\frac{Q}{Q_0}\right]\right\}. \tag{39}$$

For the gluon Sivers function, its azimuth-dependent part (in $b_\perp$ space) in the so-called Trento convention [76] is

$$f_{1T}^{\perp g(\alpha)}(x_g, b_\perp, Q) = \frac{1}{m_p}\int d^2\mathbf{k}_\perp e^{-i\mathbf{k}_\perp\cdot\mathbf{b}} k_\perp^\alpha f_{1T}^{\perp g}(x_g, k_\perp^2, Q). \tag{40}$$

Expanding this in $b_\perp$ and keeping the leading term, we get

$$f_{1T}^{\perp g(\alpha)}(x_g, b_\perp, Q) \simeq -\frac{ib_\perp^\alpha}{2m_p}\int d^2\mathbf{k}_\perp |k_\perp|^2 f_{1T}^{\perp g}(x, k_\perp^2, Q) = \frac{ib_\perp^\alpha}{2} T_{g,F}(x_g, x_g, Q). \tag{41}$$

Here $T_{g,F}(x_g, x_g, Q)$ [74,95,96] is the twist-3 Qiu-Sterman quark-gluon correlation function, treated at the leading order as a Sivers function. It is the first k_T moment term of the Sivers function and plays a significant role in the theoretical description of transverse SSAs in the framework of collinear factorization. Qiu-Sterman functions can also determine the large transverse momentum tail of gluon Sivers function. Considering Eq. (41) and the derivative of the Sivers function in $b_\perp$ space, we thus get

$$f'^{\perp g}_{1T}(x_g, b_\perp, Q) = \frac{\partial f_{1T}^{\perp g}(x_g, b_\perp)}{\partial b_\perp} = -i\frac{m_p b_\perp}{b_\perp^\alpha} f_{1T}^{\perp g(\alpha)}(x_g, b_\perp, Q) \simeq \frac{m_p b_\perp}{2} T_{g,F}(x_g, x_g, Q), \tag{42}$$

which satisfies the same evolution equation for the perturbative part as the unpolarized TMD-PDF. For the nonperturbative part, we follow Ref. [72] where the authors proposed a Sudakov form factor in the evolution formalism, which can lead to a good description of the transverse momentum distribution for different processes such as SIDIS, DY dilepton processes, and W/Z boson production in pp collisions. The nonperturbative Sudakov form factor $S_{\rm NP}$ for the Sivers function has the form

$$R_{\rm NP} = \exp\left\{-b_\perp^2\left(g_1^{\rm Sivers}+\frac{g_2}{2}\ln\frac{Q}{Q_0}\right)\right\} \tag{43}$$

where the parameter $g_1^{\rm Sivers}$ related to the averaged intrinsic transverse momenta squared $g_1^{\rm Sivers} = \langle k_{\perp s}^2\rangle_{Q_0}/4 = 0.071\ \mathrm{GeV}^2$, g_2 is universal for all different types of TMDs, is spin-independent [72], and equal to $\frac{1}{2}g_2 = 0.08\ \mathrm{GeV}^2$, and here $Q_0 = \sqrt{2.4}\ \mathrm{GeV}$ and $b_{\max} = 1.5\ \mathrm{GeV}^{-1}$. Thus, in the case of the Sivers function the evolution of its derivative can be written in the form

$$f'^{\perp g}_{1T}(x_g, b_\perp, Q_f) = f'^{\perp g}_{1T}(x_g, b_\perp, Q_i)\exp\left\{-\int_{Q_i}^{Q_f}\frac{d\mu'}{\mu'}\left(A\ln\left(\frac{Q_f^2}{\mu'^2}\right)+B\right)\right\} \times \exp\left\{-b_\perp^2\left(g_1^{\rm Sivers}+\frac{g_2}{2}\ln\frac{Q_f}{Q_0}\right)\right\}. \tag{44}$$

Setting the initial scale $Q_i = c/b_*$ and $Q_f = Q$, we finally have

$$f'^{\perp g}_{1T}(x_g, b_\perp, Q) = \frac{m_p b_\perp}{2} T_{g,F}(x_g, x_g, c/b_*) \times \exp\left\{-\int_{c/b_*}^{Q}\frac{d\mu'}{\mu'}\left(A\ln\left(\frac{Q^2}{\mu'^2}\right)+B\right)\right\} \times \exp\left\{-b_\perp^2\left(g_1^{\rm Sivers}+\frac{g_2}{2}\ln\frac{Q}{Q_0}\right)\right\}. \tag{45}$$

Here the Qiu-Sterman function $T_{g,F}(x_g, x_g, Q)$ can be parametrized proportionally to the collinear PDF as

$$T_{g,F}(x_g, x_g, Q) = N_g(x_g) f_{g/p}(x_g, Q), \tag{46}$$

with $N_g(x_g)$ defined in Eq. (20).

Therefore, the expressions for the TMDs in $k_\perp$ space can be obtained by Fourier transforming the $b_\perp$-space expressions

$$f_{g/p}(x_g,k_{\perp g},Q)=\frac{1}{2\pi}\int_0^\infty db_\perp b_\perp J_0(k_{\perp g}b_\perp)f_{g/p}(x_g,b_\perp,Q),$$
$$f_{1T}^{\perp g}(x_g,k_{\perp g},Q)=\frac{-1}{2\pi k_{\perp g}}\int_0^\infty db_\perp b_\perp J_1(k_{\perp g}b_\perp)f_{1T}^{\prime\perp g}(x_g,b_\perp,Q), \quad (47)$$

where $J_{0/1}$ are the zeroth-/first-order Bessel functions of the first kind. Using the above expressions, the asymmetry including the weighted factors $\sin(\phi_3-\phi_s)$ can be written in the TMD evolution framework as follows:

$$\frac{d\sigma^\uparrow}{d^2\mathbf{p}_3}-\frac{d\sigma^\downarrow}{d^2\mathbf{p}_3}=\int dx_\gamma d^2\mathbf{k}_{\perp\gamma}f_{\gamma/h}(x_\gamma,\mathbf{k}_{\perp\gamma})\times\frac{-1}{2\pi k_{\perp g}}\int_0^\infty db_\perp b_\perp J_1(k_{\perp g}b_\perp)f_{1T}^{\prime\perp g}(x,b_\perp,\mu)\frac{-2k_{\perp g}}{m_P}\frac{\pi}{s^2x_gx_\gamma^2}|\overline{\mathcal{M}}|^2\sin(\phi_{\perp g}-\phi_s)\sin(\phi_3-\phi_s),$$
$$\frac{d\sigma^\uparrow}{d^2\mathbf{p}_3}+\frac{d\sigma^\downarrow}{d^2\mathbf{p}_3}=2\int dx_\gamma d^2\mathbf{k}_{\perp\gamma}f_{\gamma/h}(x_\gamma,\mathbf{k}_{\perp\gamma})\frac{1}{2\pi}\int_0^\infty db_\perp b_\perp J_0(k_{\perp g}b_\perp)f_{g/p}(x_g,b_\perp,\mu)\frac{\pi}{s^2x_gx_\gamma^2}|\overline{\mathcal{M}}|^2. \quad (48)$$

III. NUMERICAL RESULTS

In this section we discuss the numerical results of the photoproduction of J/ψ by using the physical parameters $m_p=0.94$ GeV for the mass of the proton and $Q^2_{\max}=2$ GeV. The mass of the heavy quark is chosen as $m_c=1.548$ GeV. The mass of J/ψ is set to $M=2m_c$. The colliding energies used in this paper are $\sqrt{s}=115$ GeV (AFTER@LHC), $\sqrt{s}=200$ GeV (RHIC1), and $\sqrt{s}=500$ GeV (RHIC2). CTEQ6L1 [97] is used for the PDF which is probed at the factorization scale chosen as $\mu_f=M_T$, where $m_T=\sqrt{(p_T^{\mathcal{Q}})^2+m_{\mathcal{Q}}^2}$ is the $m_{\mathcal{Q}}$ transverse mass. The numerical values of the best-fit parameters of the nonperturbative Sudakov factor are given in Table I. The numerical values of the best-fit parameters for the DGLAP and TMD evolutions [26,28,31,72] at $Q_0=\sqrt{2.4}$ GeV are listed in Table II. The numerical evaluation of the Sudakov factor in the large impact parameter region at low transverse momentum is handled by the introduction of a nonperturbative function in the CSS resummation formalism. Numerical calculations are carried out using an in-house Monte Carlo generator. From Eq. (24), we symbolize the parametrizations (a) and (b) as TMD-a and TMD-b, respectively. The choices for the LDMEs for J/ψ are taken from Refs. [37,98] and shown in Table III. For $\langle 0|\mathcal{O}_8^{J/\psi}(^3P_J)|0\rangle$ with $J=1,2$, and following the heavy-quark spin symmetry, we get the relations

$$\langle 0|\mathcal{O}_8^{J/\psi}(^3P_J)|0\rangle=(2J+1)\langle 0|\mathcal{O}_8^{J/\psi}(^3P_0)|0\rangle. \quad (49)$$

In the following, we investigate the Sivers asymmetries through J/ψ photoproduction in $p^\uparrow p$ collisions with forward proton tagging. At our convenience, the Sivers asymmetry for the different kinematic variables in the DGLAP (TMD) evolution is displayed in Fig. 1 (Fig. 3) as a function of $p_T^{J/\psi}$, $y^{J/\psi}$, $\log(x_\gamma)$ and $\log(x_g)$, respectively, while in Fig. 2 (Fig. 4) it is only shown in terms of $y^{J/\psi}$. Furthermore, in Fig. 5 we analyze the single-spin asymmetry with Set I and Set II at $\sqrt{s}=115$ GeV (AFTER@LHC) in order to get the SSA uncertainty from charmonium production. The predicted SSAs are sequentially fixed for the three distinct center-of-mass energies $\sqrt{s}=115$ GeV (AFTER@LHC), $\sqrt{s}=200$ GeV (RHIC1), and $\sqrt{s}=500$ GeV (RHIC2) in Figs. 1 and 3, whereas the obtained SSAs in Figs. 2 and 4 are given for the center-of-mass energy $\sqrt{s}=115$ GeV (AFTER@LHC). The configuration of the figures is in this fashion: "SIDIS1" and "SIDIS2" are the representations of the SSAs obtained in the DGLAP evolution approach by taking into consideration the two sets of best-fit parameters SIDIS1 and SIDIS2 using the GSF fit parameters from Ref. [28]; the "BV-a"

TABLE II. Best-fit parameters of the Sivers function.

	N_a	α	β	M_1^2 GeV^2	ρ	$\langle k_\perp^2\rangle$ GeV^2	Notation
g	0.65	2.8	2.8		0.687	0.25	SIDIS1
g	0.05	0.8	1.4		0.576	0.25	SIDIS2
u	0.18	1.0	6.6	0.8		0.57	BV-a
d	−0.52	1.9	10.0	0.8		0.57	BV-b
u	0.106	1.051	4.857			0.38	TMD-a
d	−0.163	1.552	4.857			0.38	TMD-b

TABLE III. Numerical values of the LDMEs.

$\langle 0\|\mathcal{O}_{1,8}^{J/\psi}(^{2S+1}L_J)\|0\rangle$	Set I	Set II
$\langle 0\|\mathcal{O}_8^{J/\psi}(^1S_0)\|0\rangle$/GeV^3	8.9×10^{-2}	9.7×10^{-2}
$\langle 0\|\mathcal{O}_8^{J/\psi}(^3P_0)\|0\rangle$/GeV^5	1.26×10^{-2}	-2.14×10^{-2}

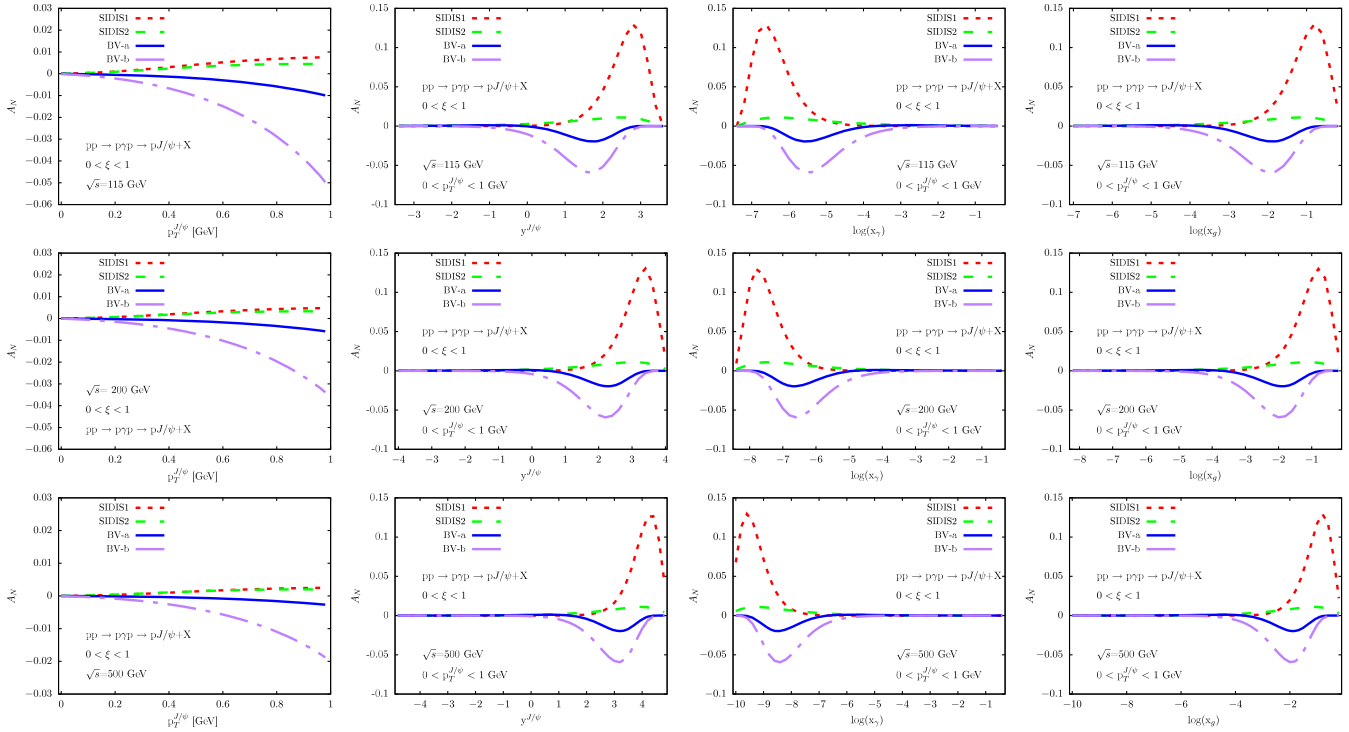

FIG. 1. Single spin asymmetry in the $pp^\uparrow \to p\gamma p^\uparrow \to p\mathcal{Q} + X$ process as a function of $p_T^{J/\psi}$ (first column), $y^{J/\psi}$ (second column), $\log(x_\gamma)$ (third column), and $\log(x_g)$ (fourth column) at $\sqrt{s} = 115$ GeV (AFTER@LHC), $\sqrt{s} = 200$ GeV (RHIC1), and $\sqrt{s} = 500$ GeV (RHIC2) using DGLAP (SIDIS1, SIDIS2, BV-a, and BV-b).

and "BV-b" plots are obtained by employing the fit parameters from Ref. [26] fit parameters.

From the hard process calculation of $c\bar{c}$ pair production through the $2 \to 1$ partonic process, it has been noticed that the Fock states are only produced in the color octet, that is to say, the asymmetry arising from J/ψ formation will be nonzero in the color-octet contribution and zero in the singlet contribution [46]. The $d\Delta\sigma$ involving the polarized cross sections and $2d\sigma$ including the unpolarized ones of Eq. (14) are computed when the initial heavy-quark pair is produced in the color-octet state. Despite the different shapes of the curves, the distinct kinematic variables in the DGLAP evolution, and being in the factorization validity in the range of x_g, the SSA decreases as the experimental center-of-mass energy increases. In the entire range of the forward-detector acceptance $0 < \xi < 1$, as shown in Figs. 1 and 2, the SSA versus $p_T^{J/\psi}$, $y^{J/\psi}$, $\log(x_\gamma)$, and $\log(x_g)$ plots have two regions of opposite signs (positive and negative) as estimated by the SIDIS and BV parameters. The asymmetries as a function of $p_T^{J/\psi}$, $y^{J/\psi}$, $\log(x_\gamma)$, and $\log(x_g)$ obtained using "SIDIS1" and "SIDIS2" parameters are positive, whereas those obtained using "BV-a" and "BV-b" parameters are negative. The sign of

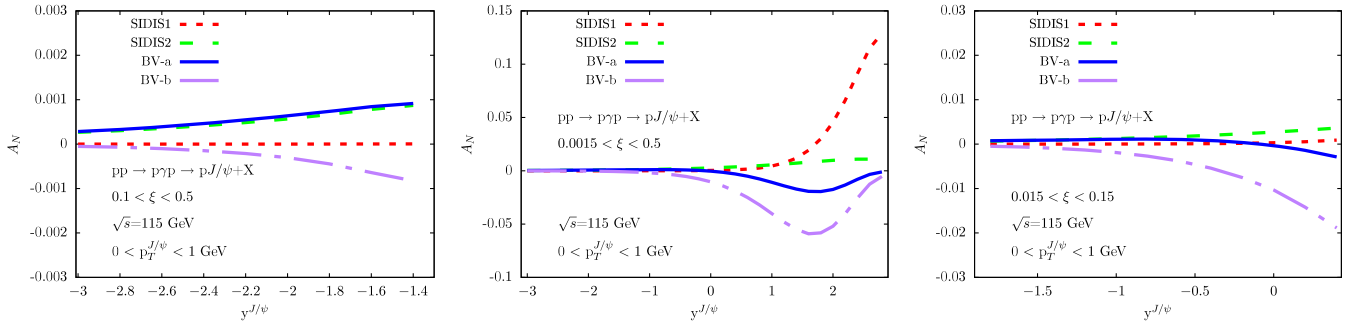

FIG. 2. Single spin asymmetry in the $pp^\uparrow \to p\gamma p^\uparrow \to p\mathcal{Q} + X$ process as a function of $y^{J/\psi}$ for $0.1 < \xi < 0.5$ (left panel), $0.0015 < \xi < 0.5$ (middle panel), and $0.015 < \xi < 0.15$ (right panel) at $\sqrt{s} = 115$ GeV (AFTER@LHC) using DGLAP evolution (SIDIS1, SIDIS2, BV-a, and BV-b).

the asymmetry depends on the relative magnitude of N_u and N_d and these have opposite sign, which can be observed in Table I. The magnitude of $N_d(x_g)$ is dominant compared to $N_u(x_g)$, and as a result the asymmetry is negative. Nevertheless, the magnitude and sign of the asymmetry strongly depends on the modeling of the GSF.

As shown in Fig. 1, the obtained asymmetry as a function of $p_T^{J/\psi}$ using "BV-a" parameters is close to zero although the center-of-mass energy is unequal, while the obtained asymmetry as a function of $y^{J/\psi}$, $\log(x_\gamma)$, and $\log(x_g)$ using "SIDIS2" parameters is close to zero despite the fact that the center-of-mass energy is also different. The obtained asymmetry as a function of $p_T^{J/\psi}$ using "BV-b" parameters is maximal around 5% at $\sqrt{s} = 115$ GeV (AFTER@LHC). We also note that the asymmetry $y^{J/\psi}$, $\log(x_\gamma)$, and $\log(x_g)$ obtained using "SIDIS1" parameters has a maximum value of around 12.5% for the three different experiments at the LHC forward-detector acceptance. We have purposefully focused on the fact that the peak SSA value is displaced positively and negatively at the right along the $y^{J/\psi}$ and $\log(x_g)$ axes, respectively, as $\sqrt{s}$ increases when the SSA is presented as a function of the rapidity and $\log(x_g)$. This is because there is a dependence between the gluon momentum fraction and the rapidity given by the formula $x_g = \frac{Me^{+y}}{\sqrt{s}}$, where M is the mass of J/ψ. The proportionality coefficient $x_g^\alpha(1-x_g)^\beta$ or Sivers effect gives the ratio of the SSA and the rapidity. Even though the same behavior is observed in the SSA versus $\log(x_\gamma)$ plot, the left displacement of the peak SSA value is negative along the axis as $\sqrt{s}$ increases. The reason is that there is also a linear correlation between the photon momentum fraction and the forward-detector acceptance ξ, and indirectly the SSA. The SSA peak displacement values of the $\log(x_\gamma)$ and $\log(x_g)$ distributions are on the left and right, respectively, but they remain negative. In DGLAP evolution, the $y^{J/\psi}$, $\log(x_\gamma)$, and $\log(x_g)$ distributions are more sensitive to measurements of SSAs than that of $p_T^{J/\psi}$, which tends to zero. We comment here that the Gaussian ansatz being $k_\perp$-dependence and factorized from x-dependence is not suitable to study SSAs [93] in the low-x_g region, and it needs to be modified to survive [99,100] as we have mentioned above.

In TMD evolution at the LHC forward-detector acceptance $0 < \xi < 1$, as seen in Fig. 3, the asymmetry with respect to $p_T^{J/\psi}$ obtained using "TMD-a" parameters is zero and positive, while the asymmetry obtained using "TMD-b" parameters is also zero and negative. At curved lines, the asymmetry slightly and positively (negatively) escapes from zero using "TMD-a" ("TMD-b" parameters). Their effects are diametrically opposite. As for the $y^{J/\psi}$, $\log(x_\gamma)$, and $\log(x_g)$ distributions, the asymmetries are negative and slightly diverge from zero. The asymmetries with regard

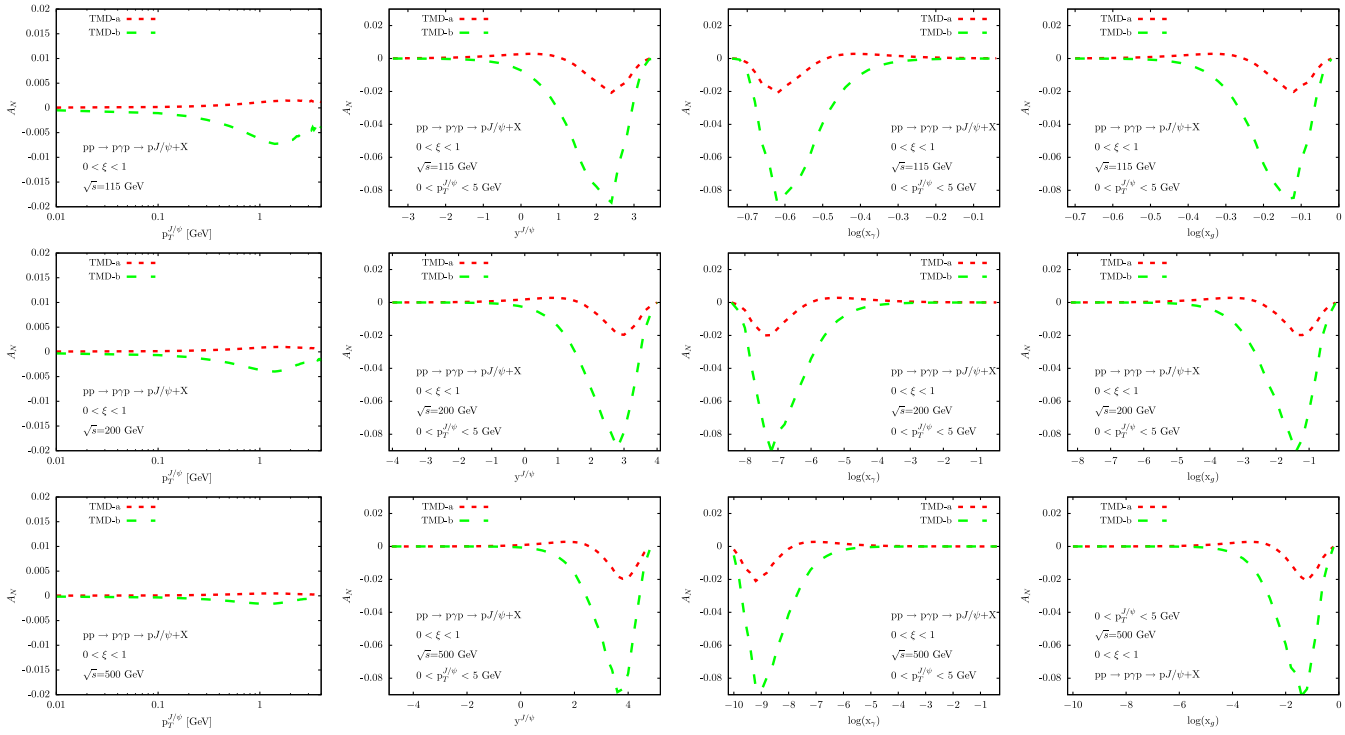

FIG. 3. Single spin asymmetry in the $pp^\uparrow \to p\gamma p^\uparrow \to p\mathcal{Q} + X$ process as a function of $p_T^{J/\psi}$ (first column), $y^{J/\psi}$ (second column), $\log(x_\gamma)$ (third column), and $\log(x_g)$ (fourth column) at $\sqrt{s} = 115$ GeV (AFTER@LHC), $\sqrt{s} = 200$ GeV (RHIC1), and $\sqrt{s} = 500$ GeV (RHIC2) using TMD evolution (TMD-a and TMD-b).

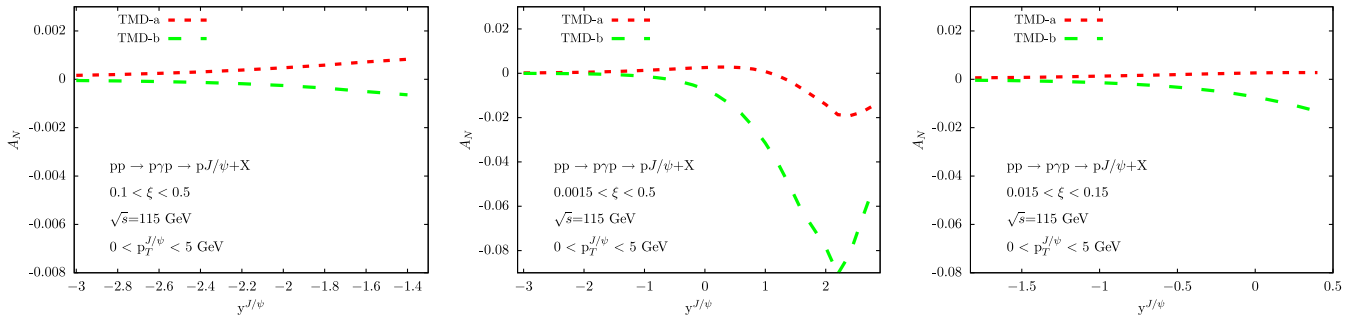

FIG. 4. Single spin asymmetry in the $pp^{\uparrow} \to p\gamma p^{\uparrow} \to p\mathcal{Q} + X$ process as a function of $y^{J/\psi}$ for $0.1 < \xi < 0.5$ (left panel), $0.0015 < \xi < 0.5$ (middle panel), and $0.015 < \xi < 0.15$ (right panel) at $\sqrt{s} = 115$ GeV (AFTER@LHC) using TMD evolution (TMD-a and TMD-b).

to $p_T^{J/\psi}$ obtained using "TMD-a" and "TMD-b" parameters are larger for the AFTER@LHC experiment ($\sqrt{s} = 115$ GeV). The displacement of the peak SSA value in TMD evolution is almost similar to that in DGLAP evolution for the plots of the obtained asymmetries versus $y^{J/\psi}$, $\log(x_\gamma)$, and $\log(x_g)$, and the asymmetry signs are also the same for the "TMD-a" and "TMD-b" parametrizations corresponding to the "BV-a" and "BV-b" parametrizations. The predicted peak SSA value in DGLAP evolution is around 12.5%, compared to that of TMD evolution which is around 7.8%.

In Fig. 2, we notice that the behaviors of the SSA versus $y^{J/\psi}$ plots in the left and right panels are utterly different due to the forward-detector acceptance range and DGLAP parametrizations. The obtained asymmetry as a function of $y^{J/\psi}$ using "BV-b" parameters is negative, and it is positive when we use "SIDIS2" and "SIDIS1" parameters for all three forward-detector acceptances. The strangeness that arises when we employ "BV-a" parameters comes from the sign change of the SSA: it is positive for the left panel, and negative for the middle and right panels. For the left and right panels, the obtained asymmetries using "SIDIS1" parameters are zero. In the right panel the asymmetry obtained using "BV-a" parameters is zero, and in the middle panel the asymmetry obtained using "SIDIS2" parameters is also zero. In the middle panel, the asymmetry as a function $y^{J/\psi}$ obtained using "SIDIS1" parameters is maximal around 12.5%.

In Fig. 4, the forward-detector acceptance range and TMD parametrizations also influence the evaluated asymmetries. The curves in the right and left panels exhibit almost the same behavior, whereas the curve in the middle panel (for the asymmetry obtained using "TMD-b" parameters) has a maximal value of around 7.8%; the asymmetries are negative when we use TMD parameters. The asymmetries in the right and left panels using "TMD-a" parameters are positive and lightly run from zero while for "TMD-b" are negative and lightly diverge from zero, too. The peak SSA values in the left and right panels of Figs. 2 and 4 occur at small rapidities, and the maxima and minima of their peak SSA values are smaller than those in the middle panels, which occur at large rapidities. The shapes, signs, and values of the SSAs in both evolutions are dissimilar because of their parametrizations.

From our calculation in Fig. 5, we show estimates of the SSAs from two different LDMEs (Set I and Set II) in DGLAP evolution as well as TMD evolution at $\sqrt{s} = 115$ GeV (AFTER@LHC) for the entire detector-acceptance range. We find that the differences between the SSAs for Set I and Set II are small, which means that the

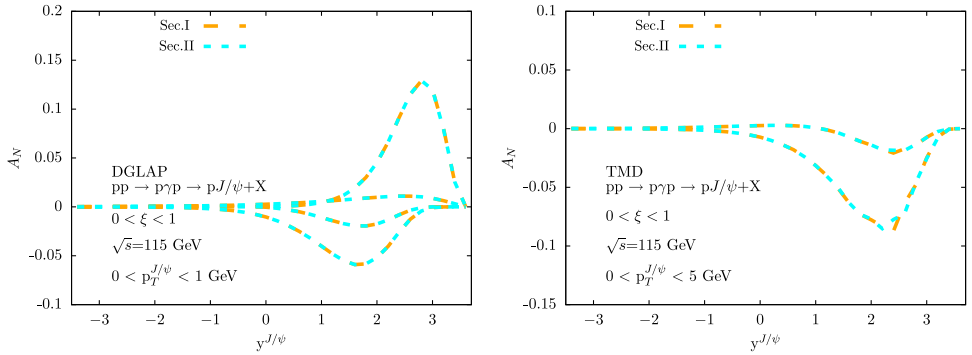

FIG. 5. Comparison of the DGLAP SSA (left panel) and TMD SSA (right panel) evaluated using Set I and Set II in the $pp^{\uparrow} \to p\gamma p^{\uparrow} \to p\mathcal{Q} + X$ process as a function of $y^{J/\psi}$ for $0 < \xi < 1$ at $\sqrt{s} = 115$ GeV (AFTER@LHC).

analyzed uncertainties are also pretty small between the two sets. Based on our numerical estimation, we find that the uncertainties are of order 10^{-3} and are thus negligible; this is understood from the fact that the SSAs are calculated through the ratio of the polarized cross sections of J/ψ photoproduction, to the unpolarized ones, and therefore the uncertainties arising from charmonium production are independent of the LDMEs or even the PDFs. The order of uncertainty also remains small at $\sqrt{s} = 200$ GeV (RHIC1) and $\sqrt{s} = 500$ GeV (RHIC2) as they are almost independent of colliding energies.

IV. SUMMARY AND DISCUSSIONS

In this paper we have evaluated the magnitude of single-spin asymmetries in the photoproduction of J/ψ by resorting to the NRQCD approach, considering both DGLAP evolution and TMD evolution. Sizable asymmetries are predicted as a function of $y^{J/\psi}$, $\log(x_\gamma)$, and $\log(x_g)$, respectively. The maximal value of the single-spin asymmetries is about 12.5% for DGLAP evolution and 7.8% for TMD evolution. The minimum and maximum of the SSAs are almost independent of energy. The obtained asymmetry as a function of $y^{J/\psi}$ and $\log(x_g)$ and the obtained asymmetry as a function of $\log(x_\gamma)$ show opposite displacement of their peaks. We chose three different forward-detector acceptances, and found that $0.0015 < \xi < 0.5$ is the region where most of the SSA effects arise and could possibly detected for both DGLAP and TMD evolutions with our choice of parametrization. In summary, our results point out that the magnitude of the asymmetries can be estimated by the photoproduction of J/ψ with forward-detector acceptances at the RHIC and AFTER@LHC experiments.

ACKNOWLEDGMENTS

H. S. is supported by the National Natural Science Foundation of China (Grant No. 11675033) and by the Fundamental Research Funds for the Central Universities (Grant No. DUT18LK27).

[1] D. L. Adams *et al.* (E581 and E704 Collaboration), Phys. Lett. B **261**, 201 (1991).
[2] D. L. Adams *et al.* (FNAL-E704 Collaboration), Phys. Lett. B **264**, 462 (1991).
[3] D. W. Sivers, Phys. Rev. D **41**, 83 (1990).
[4] X.-d. Ji, J.-P. Ma, and F. Yuan, Phys. Lett. B **597**, 299 (2004).
[5] X.-d. Ji, J.-p. Ma, and F. Yuan, Phys. Rev. D **71**, 034005 (2005).
[6] M. G. Echevarria, A. Idilbi, and I. Scimemi, J. High Energy Phys. 07 (2012) 002.
[7] A. Bacchetta, M. Diehl, K. Goeke, A. Metz, P. J. Mulders, and M. Schlegel, J. High Energy Phys. 02 (2007) 093.
[8] M. Anselmino, U. D'Alesio, and F. Murgia, Phys. Rev. D **67**, 074010 (2003).
[9] D. Boer, Phys. Rev. D **60**, 014012 (1999).
[10] S. Arnold, A. Metz, and M. Schlegel, Phys. Rev. D **79**, 034005 (2009).
[11] D. Boer, R. Jakob, and P. J. Mulders, Nucl. Phys. **B504**, 345 (1997).
[12] M. Anselmino, M. Boglione, U. D'Alesio, A. Kotzinian, F. Murgia, A. Prokudin, and C. Turk, Phys. Rev. D **75**, 054032 (2007).
[13] A. Airapetian *et al.* (HERMES Collaboration), Phys. Rev. Lett. **94**, 012002 (2005).
[14] A. Airapetian *et al.* (HERMES Collaboration), Phys. Rev. Lett. **103**, 152002 (2009).
[15] A. Airapetian *et al.* (HERMES Collaboration), Phys. Lett. B **728**, 183 (2014).
[16] C. Adolph *et al.* (COMPASS Collaboration), Phys. Lett. B **717**, 383 (2012).
[17] C. Adolph *et al.* (COMPASS Collaboration), Phys. Lett. B **736**, 124 (2014).
[18] C. Adolph *et al.* (COMPASS Collaboration), Phys. Lett. B **770**, 138 (2017).
[19] C. Adolph *et al.* (COMPASS Collaboration), Phys. Lett. B **772**, 854 (2017).
[20] M. Aghasyan *et al.* (COMPASS Collaboration), Phys. Rev. Lett. **119**, 112002 (2017).
[21] X. Qian *et al.* (Jefferson Lab Hall A Collaboration), Phys. Rev. Lett. **107**, 072003 (2011).
[22] Y. X. Zhao *et al.* (Jefferson Lab Hall A Collaboration), Phys. Rev. C **90**, 055201 (2014).
[23] L. Adamczyk *et al.* (STAR Collaboration), Phys. Rev. Lett. **116**, 132301 (2016).
[24] M. Anselmino, M. Boglione, U. D'Alesio, A. Kotzinian, F. Murgia, and A. Prokudin, Phys. Rev. D **72**, 094007 (2005); **72**, 099903(E) (2005).
[25] M. Anselmino, V. Barone, and M. Boglione, Phys. Lett. B **770**, 302 (2017).
[26] M. Anselmino, M. Boglione, U. D'Alesio, F. Murgia, and A. Prokudin, J. High Energy Phys. 04 (2017) 046.
[27] A. Martin, F. Bradamante, and V. Barone, Phys. Rev. D **95**, 094024 (2017).
[28] U. D'Alesio, F. Murgia, and C. Pisano, J. High Energy Phys. 09 (2015) 119.
[29] N. Brambilla *et al.*, Eur. Phys. J. C **71**, 1534 (2011).
[30] R. M. Godbole, A. Misra, A. Mukherjee, and V. S. Rawoot, Phys. Rev. D **85**, 094013 (2012).
[31] A. Mukherjee and S. Rajesh, Eur. Phys. J. C **77**, 854 (2017).
[32] D. Boer, Few Body Syst. **58**, 32 (2017).

[33] D. Boer, P. J. Mulders, C. Pisano, and J. Zhou, J. High Energy Phys. 08 (2016) 001.
[34] M. Anselmino, M. Boglione, U. D'Alesio, E. Leader, and F. Murgia, Phys. Rev. D **70**, 074025 (2004).
[35] U. D'Alesio, F. Murgia, C. Pisano, and P. Taels, Phys. Rev. D **96**, 036011 (2017).
[36] A. Mukherjee and S. Rajesh, Phys. Rev. D **93**, 054018 (2016).
[37] A. Mukherjee and S. Rajesh, Phys. Rev. D **95**, 034039 (2017).
[38] G. T. Bodwin, E. Braaten, and G. P. Lepage, Phys. Rev. D **51**, 1125 (1995); **55**, 5853(E) (1997).
[39] F. Abe *et al.* (CDF Collaboration), Phys. Rev. Lett. **79**, 572 (1997).
[40] D. Acosta *et al.* (CDF Collaboration), Phys. Rev. D **71**, 032001 (2005).
[41] C. Adloff *et al.* (H1 Collaboration), Eur. Phys. J. C **25**, 25 (2002).
[42] F. D. Aaron *et al.* (H1 Collaboration), Eur. Phys. J. C **68**, 401 (2010).
[43] S. Chekanov *et al.* (ZEUS Collaboration), Eur. Phys. J. C **27**, 173 (2003).
[44] H. Abramowicz *et al.* (ZEUS Collaboration), J. High Energy Phys. 02 (2013) 071.
[45] G. P. Lepage, L. Magnea, C. Nakhleh, U. Magnea, and K. Hornbostel, Phys. Rev. D **46**, 4052 (1992).
[46] F. Yuan, Phys. Rev. D **78**, 014024 (2008).
[47] S. Rajesh, R. Kishore, and A. Mukherjee, Phys. Rev. D **98**, 014007 (2018).
[48] R. M. Godbole, A. Misra, A. Mukherjee, and V. S. Rawoot, Phys. Rev. D **88**, 014029 (2013).
[49] R. M. Godbole, A. Kaushik, A. Misra, and V. S. Rawoot, Phys. Rev. D **91**, 014005 (2015).
[50] D. Boer, C. Lorcé, C. Pisano, and J. Zhou, Adv. High Energy Phys. **2015**, 1 (2015).
[51] R. M. Godbole, A. Kaushik, and A. Misra, Phys. Rev. D **94**, 114022 (2016).
[52] D. Boer and W. Vogelsang, Phys. Rev. D **69**, 094025 (2004).
[53] T. C. Rogers and P. J. Mulders, Phys. Rev. D **81**, 094006 (2010).
[54] M. G. Albrow *et al.* (FP420 R, D Collaboration), J. Instrum. **4**, T10001 (2009).
[55] V. P. Goncalves, Phys. Rev. D **97**, 014001 (2018).
[56] V. M. Budnev, I. F. Ginzburg, G. V. Meledin, and V. G. Serbo, Phys. Rep. **15**, 181 (1975).
[57] G. Baur, K. Hencken, D. Trautmann, S. Sadovsky, and Y. Kharlov, Phys. Rep. **364**, 359 (2002).
[58] A. Petrelli, M. Cacciari, M. Greco, F. Maltoni, and M. L. Mangano, Nucl. Phys. **B514**, 245 (1998).
[59] M. Cacciari and M. Krämer, Phys. Rev. Lett. **76**, 4128 (1996).
[60] U. D'Alesio and F. Murgia, Phys. Rev. D **70**, 074009 (2004).
[61] P. Schweitzer, T. Teckentrup, and A. Metz, Phys. Rev. D **81**, 094019 (2010).
[62] W. Broniowski and E. Ruiz Arriola, Phys. Rev. D **97**, 034031 (2018).
[63] X. Yao, Y. Hagiwara, and Y. Hatta, Phys. Lett. B **790**, 361 (2019).
[64] S. Melis, EPJ Web Conf. **85**, 01001 (2015).
[65] F. Landry, R. Brock, P. M. Nadolsky, and C. P. Yuan, Phys. Rev. D **67**, 073016 (2003).
[66] A. V. Konychev and P. M. Nadolsky, Phys. Lett. B **633**, 710 (2006).
[67] J. Collins, L. Gamberg, A. Prokudin, T. C. Rogers, N. Sato, and B. Wang, Phys. Rev. D **94**, 034014 (2016).
[68] A. Bacchetta, F. Delcarro, C. Pisano, M. Radici, and A. Signori, J. High Energy Phys. 06 (2017) 081.
[69] J. C. Collins, D. E. Soper, and G. F. Sterman, Nucl. Phys. **B250**, 199 (1985).
[70] J.-w. Qiu and X.-f. Zhang, Phys. Rev. Lett. **86**, 2724 (2001).
[71] J.-w. Qiu and X.-f. Zhang, Phys. Rev. D **63**, 114011 (2001).
[72] M. G. Echevarria, A. Idilbi, Z.-B. Kang, and I. Vitev, Phys. Rev. D **89**, 074013 (2014).
[73] A. Bacchetta and A. Prokudin, Nucl. Phys. **B875**, 536 (2013).
[74] Z.-B. Kang, B.-W. Xiao, and F. Yuan, Phys. Rev. Lett. **107**, 152002 (2011).
[75] M. G. Echevarria, A. Idilbi, A. Schäfer, and I. Scimemi, Eur. Phys. J. C **73**, 2636 (2013).
[76] S. M. Aybat, J. C. Collins, J.-W. Qiu, and T. C. Rogers, Phys. Rev. D **85**, 034043 (2012).
[77] D. Boer and W. J. den Dunnen, Nucl. Phys. **B886**, 421 (2014).
[78] S. Catani, E. D'Emilio, and L. Trentadue, Phys. Lett. B **211**, 335 (1988).
[79] R. P. Kauffman, Phys. Rev. D **45**, 1512 (1992).
[80] A. Idilbi, X.-d. Ji, and F. Yuan, Nucl. Phys. **B753**, 42 (2006).
[81] D. de Florian and M. Grazzini, Phys. Rev. Lett. **85**, 4678 (2000).
[82] D. de Florian and M. Grazzini, Nucl. Phys. **B616**, 247 (2001).
[83] P. Sun, C. P. Yuan, and F. Yuan, Phys. Rev. D **88**, 054008 (2013).
[84] M. Beneke, Phys. Rep. **317**, 1 (1999).
[85] C. T. H. Davies, B. R. Webber, and W. J. Stirling, Nucl. Phys. **B256**, 413 (1985).
[86] A. S. Ito *et al.*, Phys. Rev. D **23**, 604 (1981).
[87] D. Antreasyan *et al.*, Phys. Rev. Lett. **47**, 12 (1981).
[88] D. Antreasyan *et al.*, Phys. Rev. Lett. **48**, 302 (1982).
[89] G. A. Ladinsky and C. P. Yuan, Phys. Rev. D **50**, R4239 (1994).
[90] F. Landry, R. Brock, G. Ladinsky, and C. P. Yuan, Phys. Rev. D **63**, 013004 (2000).
[91] S. M. Aybat and T. C. Rogers, Phys. Rev. D **83**, 114042 (2011).
[92] J. C. Collins and D. E. Soper, Nucl. Phys. **B284**, 253 (1987).
[93] P. Sun, J. Isaacson, C. P. Yuan, and F. Yuan, Int. J. Mod. Phys. A **33**, 1841006 (2018).
[94] Z.-B. Kang, X. Liu, F. Ringer, and H. Xing, J. High Energy Phys. 11 (2017) 068.
[95] Z.-B. Kang, J.-W. Qiu, W. Vogelsang, and F. Yuan, Phys. Rev. D **83**, 094001 (2011).
[96] C. Kouvaris, J.-W. Qiu, W. Vogelsang, and F. Yuan, Phys. Rev. D **74**, 114013 (2006).

[97] J. Pumplin, D. R. Stump, J. Huston, H. L. Lai, P. M. Nadolsky, and W. K. Tung, J. High Energy Phys. 07 (2002) 012.
[98] K.-T. Chao, Y.-Q. Ma, H.-S. Shao, K. Wang, and Y.-J. Zhang, Phys. Rev. Lett. **108**, 242004 (2012).
[99] P. M. Nadolsky, D. R. Stump, and C. P. Yuan, Phys. Rev. D **61**, 014003 (1999); **64**, 059903(E) (2001).
[100] P. M. Nadolsky, D. R. Stump, and C. P. Yuan, Phys. Rev. D **64**, 114011 (2001).